THE JOURNAL OF PHYSICAL CHEMISTRY C

Article

Cite This: J. Phys. Chem. C 2019, 123, 24705−24713

pubs.acs.org/JPCC

Theoretical Study of the Mechanism of Aggregation-Caused Quenching in Near-Infrared Thermally Activated Delayed Fluorescence Molecules: Hydrogen-Bond Effect

Kai Zhang, Jie Liu, Yuchen Zhang, Jianzhong Fan, Chuan-Kui Wang,* and Lili Lin*

Shandong Province Key Laboratory of Medical Physics and Image Processing Technology, School of Physics and Electronics, Shandong Normal University, 250014 Jinan, China

Supporting Information

ABSTRACT: Aggregation-caused quenching (ACQ) has long been a problem that inhibits the application of organic light-emitting materials in organic light-emitting diodes, especially near-infrared (NIR) materials. Figuring out the reasons that induce ACQ is important for the quantum efficiency enhancement of NIR materials. In this paper, an NIR molecule (TPA-QCN) with thermally activated delayed fluorescence (TADF) is studied based on first-principles calculations and excited-state dynamics investigation in both toluene and in the aggregation state. Our calculation indicates that aggregation can induce a smaller energy gap between the first singlet excited state and the first triplet excited state, which is favorable for TADF. Both the decreased fluorescent rate and the increased nonradiative rate will induce emission quenching in the aggregation state. Based on detailed analyses of the reorganization energy and intermolecular interaction, we find that the hydrogen bond will induce enhanced contribution to the reorganization energy from C−H stretching vibration modes and thus a larger nonradiative rate in the aggregation state than in toluene. A new mechanism of ACQ is proposed, and it could help in the design of new types of NIR-TADF molecules with enhanced fluorescence efficiency.

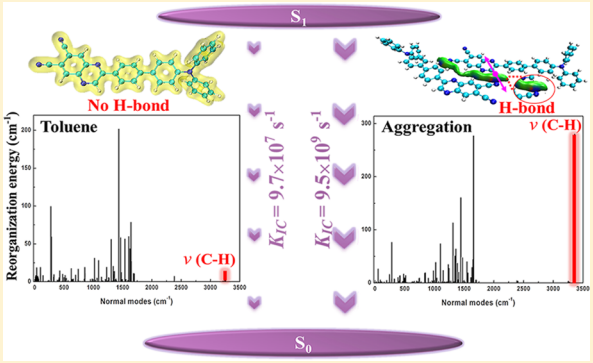

1. INTRODUCTION

Thermally activated delayed fluorescence (TADF) molecules, which are thought as the third-generation light-emitting materials in organic light-emitting diodes (OLED), can harvest both singlet and triplet excited states for luminescence through an efficient reverse intersystem crossing (RISC) process, and significant progress has been achieved.[1−11] Although several hundreds of TADF molecular materials have been synthesized and reported, deep red (DR) or near-infrared (NIR) TADF materials are still quite limited and new design strategies are urgently need.[12−15] Most of the DR or NIR-TADF molecules show efficient emission when they are dissolved or dispersed in solvents. Their application in OLEDs is still quite difficult, since most of the DR or NIR molecules cannot avoid the aggregation-caused quenching (ACQ) problem.[16,17] To obtain highly efficient NIR-TADF molecules in OLEDs, the aggregation effect on the light-emitting properties of molecules should be revealed first. As far as we know, H-aggregation is often thought as the reason that induces ACQ, and avoiding the generation of H-aggregation in the aggregation state is usually adopted to enhance the light-emitting efficiency of molecules by molecular engineering. However, ACQ could not be avoided although H-aggregation no longer existed in the solid film.[18,19] Consequently, the ACQ mechanism of NIR emitters should be further explored to favor its design.

In this paper, an NIR-TADF molecule with heterocyclic quinoxaline-6,7-dicarbonitrile (QCN) as the acceptor (A) and bulky triphenylamine (TPA) as the donor (D) (TPA−QCN) is studied as a model (with the structure shown in Figure 1a). The molecule TPA−QCN was first synthesized and reported by Wang' group, and high efficiency in the aggregation state was obtained due to the reduction of face-to-face accumulation and the formation of J-aggregation.[19] Nevertheless, ACQ was not totally eliminated in the aggregation state. H-aggregation should not be the sole cause that induces quenching in the aggregation state. Here, we performed a systematic study of the light-emitting properties of TPA−QCN molecules in both solvent and in crystals to figure out the reason for ACQ. The results would provide new insights on the ACQ mechanism and help in the design of high-efficiency NIR-TADF molecules in the aggregation state.

2. THEORETICAL METHODS

Since light-emitting properties of organic molecules are closely related to the excited states, the optimization of excited states is performed using the time-dependent density functional

Received: July 4, 2019
Revised: September 6, 2019
Published: September 18, 2019

DOI: 10.1021/acs.jpcc.9b06388
J. Phys. Chem. C 2019, 123, 24705−24713

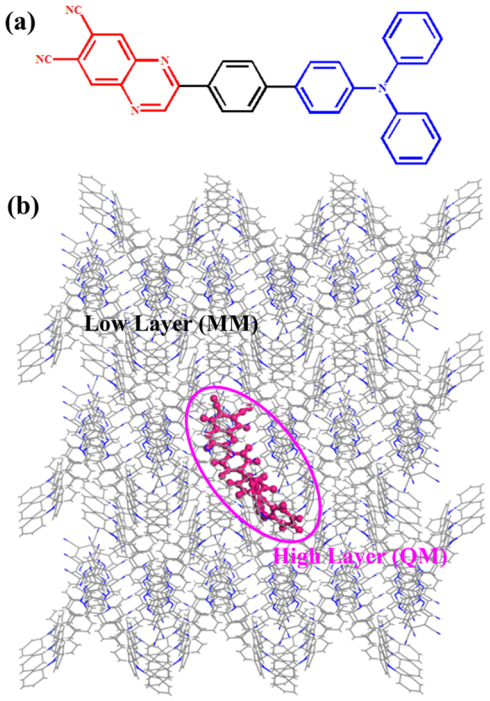

Figure 1. (a) Geometry structure of the studied molecule TPA−QCN. (b) ONIOM model: the centered molecule is treated as a high layer and the surrounding molecules are fixed as the low layer.

theory (TD-DFT). The ground states are optimized with the density functional theory (DFT). No virtual frequency for normal vibration modes is found in optimized structures, which confirmed the stability of the geometry obtained. To simulate the toluene solvent, the polarizable continuous solvent model is used, which has been proven to be reliable to predict the solvent effect on TADF molecules.[20−23] To simulate molecular properties in the aggregation state, the combined quantum mechanics and molecular mechanics (QM/MM) method is adopted. Here, the two-layer ONIOM model is used (as shown in Figure 1b). The packing structure of TPA−QCN in a crystal is set as the initial configuration for the ONIOM model. In this model, one molecule is chosen as the high layer and calculated with the QM method. The other molecules are set as the low layer and are treated with the MM method. For the MM calculation, the universal force field is adopted.[24−29] For the QM calculations, the TD-DFT method is used and the electronic embedding mechanism is adopted to treat the QM/MM interaction. The MM charges were incorporated into the one-electron part of the QM Hamiltonian, and the QM/MM electrostatic interactions were evaluated from the QM electrostatic potential and the MM partial charges. Since TPA−QCN is a typical D−A molecule whose excited states are sensitive to functionals, several functionals with different Hartree Fork components or with separate short- and long-range interactions are tested according to the fluorescence emission wavelengths (as listed in Table 1). It is found that the emission wavelength changes significantly when functionals are different. The value calculated with PBE0 in the aggregation state is in good agreement with the experimental values. Thus, PBE0 is adopted in all of the following QM calculations in this work. Besides, the 6-31G* basis set is used. All of the calculations above are realized in the Gaussian 16 program.[30]

Table 1. Emission Wavelengths Calculated with Different Functionals for TPA−QCN in Toluene and in the Aggregation State (Unit: nm)

	toluene	aggregation
B3LYP	758	847
PBE0	664	733
BMK	503	523
M062X	462	449
CAM-B3LYP	452	433
ωB97XD	437	412
Exp[a]	585	733

[a]Exp is experimental data.

The fluorescence efficiency $\left(\Phi_F = \frac{k_r}{k_r + k_{nr}}\right)$, which relies on the competition between the radiative rate (k_r) and the nonradiative rate (k_{nr}), is an important parameter that determines the quantum efficiency of OLEDs.[31−33] k_{nr} is generally a sum of the internal conversion rate (k_{IC}) and the intersystem crossing rate (k_{ISC}). k_r is the fluorescence rate, which can be calculated with the Einstein's spontaneous emission equation

$$k_r = \frac{f \Delta E_{fi}^2}{1.499\ \mathrm{cm}^{-2}\cdot\mathrm{s}} \tag{1}$$

Here, f is the oscillator strength of the first singlet excited state (S_1) and ΔE_{fi} in units of wavenumber (cm^{-1}) is the energy difference between S_1 and the ground state (S_0). k_{IC} is the nonradiative internal rate, which was deduced based on Fermi's golden rule and the first-order perturbation theory, and it can be written as follows

$$k_{IC} = \sum_{kl} \frac{1}{\hbar^2} R_{kl} \int_{-\infty}^{\infty} \mathrm{d}t [e^{i\omega_{ij}t} Z_i^{-1} \rho_{IC}(t, T)] \tag{2}$$

Here, $R_{kl} = \langle \Phi_f | P_{fk} | \Phi_i \rangle \langle \Phi_i | P_{fi} | \Phi_f \rangle$ is the nonadiabatic electronic coupling, Z_i is the partition function, and $\rho_{IC}(t, T) = Tr(\hat{P}_{fk} e^{-i\tau_f \hat{H}_f} \hat{P}_{fl} e^{-i\tau_i \hat{H}_i})$ is the thermal vibration correlation function (TVCF).[34−36]

Similarly, the intersystem crossing (ISC) rate and reverse intersystem crossing (RISC) rate between two electronic states with different spin multiplicities are calculated using the Marcus rate equation

$$k_{ji} = \frac{V_{ji}^2}{\hbar} \sqrt{\frac{\pi}{k_B T \lambda}} \cdot \exp\left[-\frac{(\Delta G_{ji} + \lambda)^2}{4\lambda k_B T}\right] = \frac{V_{ji}^2}{\hbar} \sqrt{\frac{\pi}{k_B T \lambda}} \cdot \exp\left[-\frac{\Delta G^{\perp}}{k_B T}\right] \tag{3}$$

Here, k_B is the Boltzmann constant and T is the temperature, which is set as 300 K. V_{ji} represents the spin orbit coupling, which is calculated by the quadratic response function method in the Dalton program.[37] In the active energy, ΔG_{ji} represents the energy difference between S_1 and the first triplet excited state (T_1), and λ is the reorganization of the S_1 and T_1 involved. For the calculation of the ISC rate, $\Delta G_{ji} = E_{T_1} - E_{S_1}$.

To characterize the intermolecular interaction in the aggregation state, the independent gradient model (IGM) is adopted.[38] In this method, the δg function defined as the subtraction between the initial molecular density gradient $g(r)$ and $g^{IGM}(r)$ is used

DOI: 10.1021/acs.jpcc.9b06388
J. Phys. Chem. C 2019, 123, 24705−24713

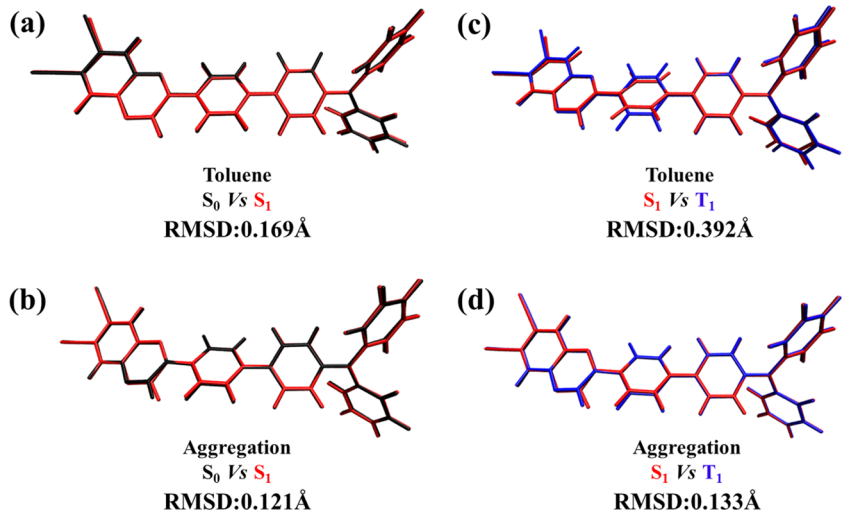

Figure 2. Geometry comparison and RMSD values between S_0 (black), S_1 (red), and T_1 (blue) in toluene (a, c) and in the aggregation state (b, d).

$$\delta g(r) = g^{\mathrm{IGM}}(r) - g(r) \tag{4}$$

$$g(r) = \left| \sum_i \nabla \rho_i(r) \right| \tag{5}$$

$$g^{\mathrm{IGM}}(r) = \left| \sum_i \mathrm{abs}[\nabla \rho_i(r)] \right| \tag{6}$$

where i is the atomic ordinal number and $\nabla\rho(r)$ is the gradient vector; abs$(\nabla\rho)(r)$ represents that every component of $\nabla\rho(r)$ vector takes the absolute value. Besides, based on the molecular force field energy decomposition method, various weak interactions can be characterized by Multiwfn.[39] The electrostatic, exchange repulsion, and dispersion interaction energies between the atoms used the potential form for most of the molecular force fields. The corresponding formula is written as follows

$$E_{\mathrm{AB}}^{\mathrm{ele}} = \frac{q_{\mathrm{A}} q_{\mathrm{B}}}{r_{\mathrm{AB}}} \tag{7}$$

$$E_{\mathrm{AB}}^{\mathrm{rep}} = \varepsilon_{\mathrm{AB}} \left(\frac{R_{\mathrm{AB}}^0}{r_{\mathrm{AB}}} \right)^{12} \tag{8}$$

$$E_{\mathrm{AB}}^{\mathrm{disp}} = -2\varepsilon_{\mathrm{AB}} \left(\frac{R_{\mathrm{AB}}^0}{r_{\mathrm{AB}}} \right)^{6} \tag{9}$$

where A and B represent two atoms, and q, r, and ε represent the atomic charge, distance between two atoms, and the depth of van der Waals potential well, respectively.

3. RESULTS AND DISCUSSION

3.1. Geometry and Electronic Structures. First, we optimized the geometry of the ground and excited states of the molecule in toluene and in the aggregation state and compared the geometric changes between different states by root mean square displacement (RMSD) values using Multiwfn (as shown in Figure 2). The molecular geometry optimized in toluene is different from that optimized in the aggregation state. From the RMSD of S_0, S_1, and T_1, we find that the difference is mainly located at the dihedral angle between the accepter and the benzene ring. It is also found that the RMSD values in excited states are larger than those in the ground state, which means that excited states are more sensitive to the environment. It can be easily seen that the geometric change between S_0 and S_1 is also mainly located at the accepter and π conjugate chain in toluene (RSMD = 0.169 Å) (as shown in Figure 2a). The change in the aggregation state is obviously limited with RMSD = 0.121 Å (as shown in Figure 2b). It indicates that the intermolecular interaction can inhibit molecular geometry changes when the molecule is excited in the aggregation state. In addition, the RMSD value between S_0 and T_1 in the aggregation state (0.133 Å) is much smaller than that in toluene (0.392 Å) (as shown in Figure 2d,c). It further indicates that molecular geometric variation can be effectively limited in the aggregation state when the molecules are excited, which may induce less nonradiative energy and achieve effective luminescence.

The electron distributions of the highest occupied molecular orbitals (HOMOs) and lowest unoccupied molecular orbitals (LUMOs) are shown in Figure 3. It is found that electrons in HOMOs are mainly distributed at the donor unit, while those of LUMOs are mostly located at the acceptor unit. The effective separation of the HOMO and LUMO is beneficial to

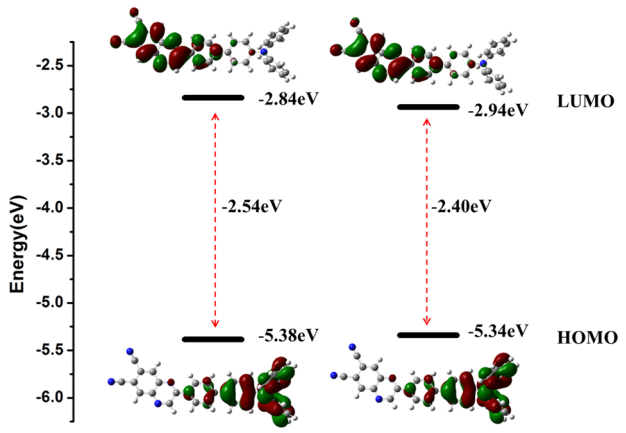

Figure 3. Energy and electron distribution of HOMOs and LUMOs for a molecule in toluene and in the aggregation state (isovalue = 0.02).

DOI: 10.1021/acs.jpcc.9b06388
J. Phys. Chem. C 2019, 123, 24705−24713

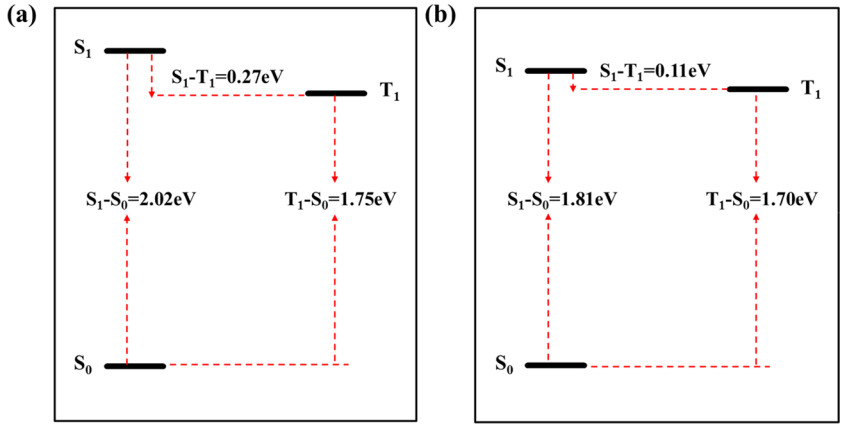

Figure 4. Energy levels of three low-lying states for TPA−QCN calculated based on the optimized geometry in toluene (a) and in the aggregation state (b), respectively.

the production of a small energy gap between S_1 and T_1. In addition, the energy level of the HOMO in the aggregation state (−5.34 eV) is 0.04 eV higher than that in toluene (−5.38 eV), while the LUMO energy level in the aggregation state (−2.94 eV) is 0.1 eV lower than that in toluene (−2.84 eV). Aggregation results in the HOMO−LUMO gap becoming narrower, and thus in a red shift of the emission compared with that in toluene, which is consistent with the experimental results.

3.2. Excited-State Properties. For TADF molecules, the energy gap between S_1 and T_1 (ΔE_{ST}) plays an important role in the RISC process. Thus, the adiabatic excitation energies of low-lying excited states for the TPA−QCN molecule in toluene and in the aggregation state are shown in Figure 4. The energy levels of S_1 and T_1 are both lowered in the aggregation state than in toluene with the reduction of S_1 being more significant, and thus a smaller ΔE_{ST} is obtained in the aggregation state. The ΔE_{ST} values for the molecule in toluene and in the aggregation state are 0.27 and 0.11 eV, respectively, which indicate that the aggregation state can reduce ΔE_{ST}. In addition, the transition properties of related excited states are illustrated in Figure 5. The local excitation (LE) state with a large orbital overlap is favorable for efficient radiation. However, the electronic transition for the charge transfer (CT) state is prohibited by the complete spatial separation of the transition orbits, and the fluorescence efficiency is often very low. The hybridized local and charge-transfer (HLCT) excited state is a mixed state with both LE and CT properties.[40] The natural transition orbitals (NTO) of both S_1 and T_1 obtained in toluene and in the aggregation state are illustrated in Figure 5a,b. The percentage in the figures represents the proportion of the local excitation component in the transition, and the CT (0−40%), HLCT (40−75%), and LE (75−100%) characteristics of both singlet and triplet excited states are quantitatively classified.[41] S_1 is a typical CT state with the highest occupied natural transition orbital (HONTO) localized in TPA and the lowest unoccupied natural transition orbital (LUNTO) mainly concentrated at QCN, whether it is in toluene or in the aggregation state. However, T_1 in both phases are HLCT states, and there was a significant overlap in the conjugation chain between HONTO and LUNTO. In addition, the CT contribution to the transition in both S_1 and T_1 in the aggregation state is obviously increased compared with that in toluene. In theory, the CT states tend to form a small ΔE_{ST}.[42] Our calculation results are consistent with the theory.

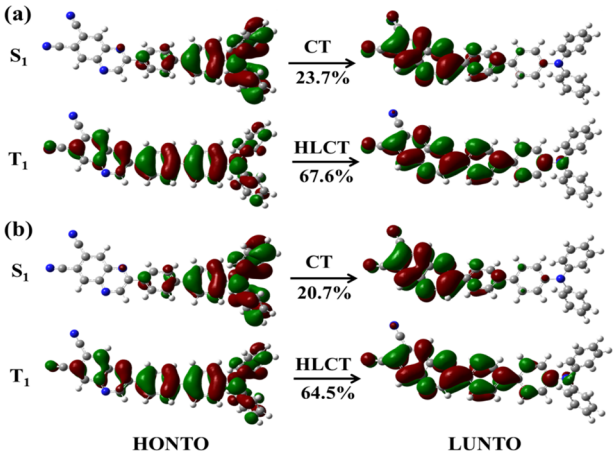

Figure 5. Transition characteristics for singlet and triplet sates of TPA−QCN in toluene (a) and in the aggregation state (b) respectively (isovalue = 0.02). The values below the arrows are the LE proportion in excitation.

3.3. Decay Rates of Excited States. Based on the energy levels of excited states, the excited-state dynamics of TPA−QCN are investigated, and the corresponding data are listed in Table 2. The ISC and RISC processes are not only related to ΔE_{ST}, but also have a relationship with the spin orbit coupling (SOC) constants between S_1 and T_1. The SOC values calculated both in toluene and in the aggregation state are also shown in Table 2. It can be seen that the calculated ISC rate in the aggregation state (7.19×10^6 s^{-1}) is smaller than that in toluene (1.05×10^7 s^{-1}), which should be caused by the larger SOC constant (0.162 cm^{-1}) in toluene. As for the RISC rate, the value in the aggregation state (1.79×10^5 s^{-1}) is about 3 orders of magnitude larger than that in toluene (2.45×10^2 s^{-1}). This is not only related to the smaller energy difference in the aggregation state, but also a result of the larger SOC constant (0.225 cm^{-1}). Moreover, the radiative decay rate in the aggregation state (2.10×10^7 s^{-1}) is smaller than that in toluene (3.78×10^7 s^{-1}), while the calculation of the transition dipole moments of the molecule in the aggregation state and toluene are 6.82 and 6.80 D, respectively. According to Einstein's spontaneous emission equation, the main factor of the decrease of the radiative decay rate is attributed to the

DOI: 10.1021/acs.jpcc.9b06388
J. Phys. Chem. C 2019, 123, 24705−24713

Table 2. Radiative and Nonradiative Rates of S_1 as well as the Spin−Orbit Coupling (SOC), Intersystem Crossing (ISC), and Reverse Intersystem Crossing (RISC) Rates between S_1 and T_1[d]

		SOC[a] (cm^{-1})	k_{ISC} (s^{-1})	SOC[b] (cm^{-1})	k_{RISC} (s^{-1})	k_r (s^{-1})	k_{IC} (s^{-1})	Φ_F
toluene	S_1-S_0					3.78×10^7	9.70×10^7	26.11%
	Exp[c]					3.83×10^7	7.11×10^7	34.1%
	S_1-T_1	0.162	1.05×10^7	0.156	2.45×10^2			
	Exp[c]		0.29×10^7		2.00×10^2			
aggregation	S_1-S_0					2.10×10^7	9.51×10^9	0.22%
	Exp[c]					1.38×10^7	5.19×10^7	19.7%
	S_1-T_1	0.156	7.19×10^6	0.225	1.79×10^5			
	Exp[c]		4.40×10^6		0.53×10^5			

[a]Notes: calculated based on the optimized geometry of S_1. [b]Calculated based on the optimized geometry of T_1. [c]Exp. represented experimental data. [d]Fluorescence efficiency (Φ_F) calculated is listed.

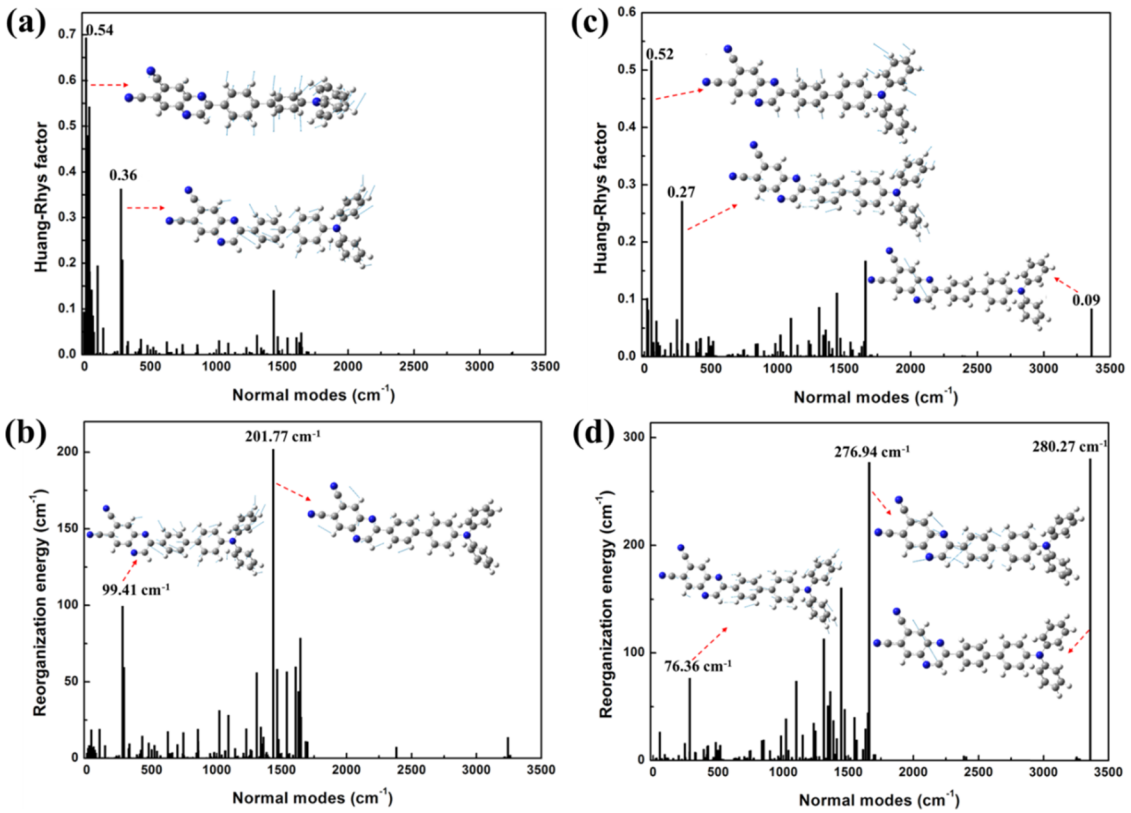

Figure 6. Calculated HR factors versus the normal mode frequencies in toluene (a) and in the aggregation state (c) as well as the reorganization energies versus the normal mode frequencies in toluene (b) and in the aggregation state (d) respectively. Representative vibration modes are shown as insets.

decrease of energy difference between S_1 and S_0 in the aggregation state (1.81 eV) compared with that in toluene (2.02 eV). Besides, the calculated nonradiative internal decay rate k_{IC} in the aggregation state (9.51×10^9 s^{-1}) is about 2 orders of magnitude larger than that in toluene (9.70×10^7 s^{-1}). Based on the decay rates, the fluorescence efficiencies of the molecule in solvent and in the aggregation state are calculated. It can be seen that the fluorescence efficiency in the aggregation state (Φ_F = 0.22%) is significantly lower than that in the solvent (Φ_{PF} = 26.11%), and the ACQ phenomenon is confirmed. Although a decrease in the radiative rate is one reason that induces ACQ, the increase of the nonradiative rate should play the main role. In addition, we can find that the calculated values in toluene are in good agreement with the experimental values. In aggregation, the calculated rates except the internal conversion rate are also in good agreement with the experimental values. The fact that the difference between the calculated internal conversion rate and the experimental result should be due to different environments is considered in the calculation. The experimental result is obtained for the doping film, while the theoretical calculation is performed based on a crystal structure. Thus, different aggregation environments are involved, especially for the hydrogen bonds.

3.4. Intermolecular Interaction. To make out the reason that induced the larger nonradiative rate in the aggregation state, the HR factors and reorganization energy closely related to the nonradiative rate for every vibration mode are calculated and shown in Figure 6. The reorganization energy (λ) can be expressed as a sum of the contributions from normal mode analysis in the harmonic oscillator approximation

DOI: 10.1021/acs.jpcc.9b06388
J. Phys. Chem. C 2019, 123, 24705−24713

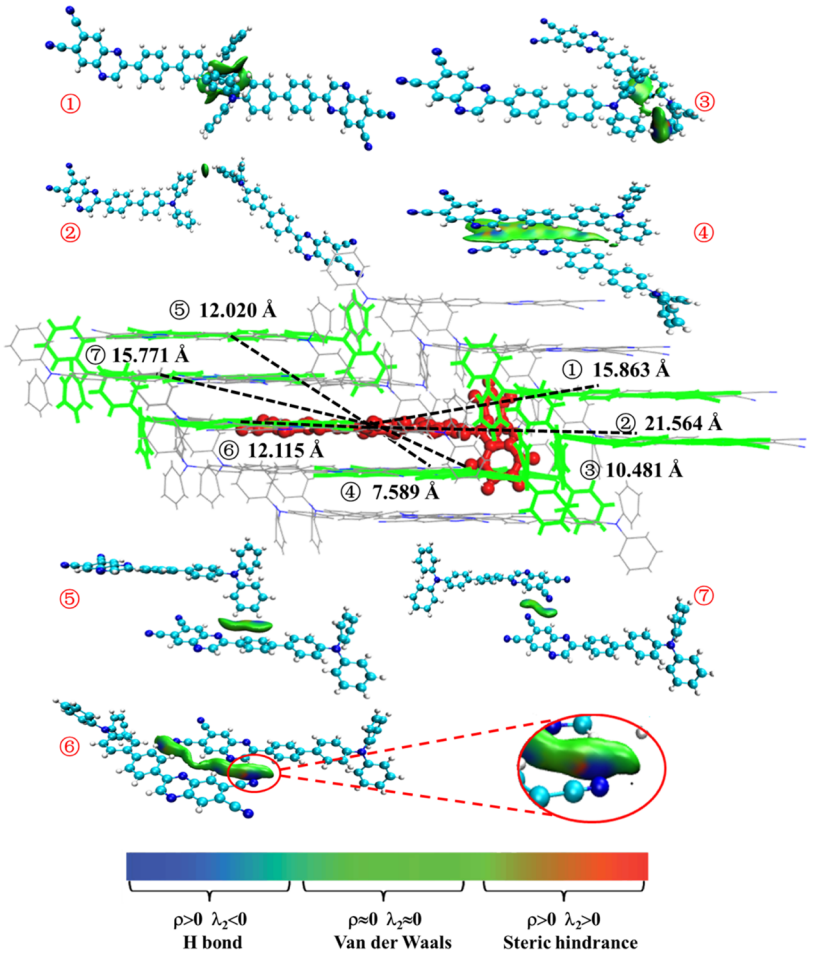

Figure 7. Intermolecular interactions for several dimers described by the IGM method.

$$\lambda_{gs} = \sum_{k\in gs} \lambda_k = \sum_{k\in gs} \hbar\omega_k \mathrm{HR}_k \tag{10}$$

$$\lambda_{es} = \sum_{k\in es} \lambda_k = \sum_{k\in es} \hbar\omega_k \mathrm{HR}_k \tag{11}$$

$$\mathrm{HR}_k = \frac{\omega_k {D_k}^2}{2\hbar} \tag{12}$$

In the equation above, HR_k is the Huang−Rhys factor for the kth mode and D_k represents the displacement for mode k between the equilibrium geometries of S_0 and S_1. This is can be realized with the DUSHIN module in MOMAP.[43] It is found that the HR factors in toluene are mainly contributed by low-frequency modes (such as HR = 0.54 and 0.36), and they mainly correspond to the rotation of the donor and conjugate chains (see the insets in Figure 6a). For the HR factors in the aggregation state, the contribution from low-frequency modes decreases slightly (such as HR = 0.52 and 0.27), while a relative large HR factor (HR = 0.09) from the high-frequency mode shows up. By a detailed analysis, we found that the high-frequency mode corresponds to the C−H stretching mode (see the insets in Figure 6c). Furthermore, we find that the contribution to the reorganization energy of low-frequency modes (1−500 cm^{-1}) is reduced by 71 cm^{-1} in the aggregation state. The vibration modes with moderate frequency (500−1500 cm^{-1}) contribute more to the reorganization energy (429 cm^{-1}) in the aggregation state. The contribution form the C−H vibration mode is also increased in the aggregation state. The total reorganization energy for TPA−QCN in toluene is about 1287 cm^{-1}, while it is increased to 1916 cm^{-1}. The contribution of the C−H stretching vibration mode to the reorganization energy is 280 cm^{-1}, which shows an important role of the increase of the total reorganization energy (629 cm^{-1}). Here, we should notice that different influence results of aggregation are found for the RMSD values and reorganization energy. The aggregation could induce decreased RMSD values, but an increased reorganization energy. This is due to the different relationships between RMSD values or reorganization energies and the geometries. From Table S1 and Figure S1, we can see that the dihedral angles have a more obvious change than bond lengths when the molecule is excited from S_0 to S_1. Thus, RMSD values mainly reflect on the variation of dihedral angles. However, the reorganization energy is mainly contributed by vibrations involving bond lengths.[28,29] Since the vibration modes with low frequency come from the rotation of donor groups, which reflect the change of dihedral angles, the decreased change of dihedral angles will induce a reduced reorganization energy from low-frequency modes. This is consistent with our calculation results.

Based on the analysis above, we think that the C−H stretching vibration mode plays an important role in the increase of the reorganization energy, and the contribution proportion is about 44.5%. We wondered as to why the C−H stretching mode shows enhanced contribution to the

DOI: 10.1021/acs.jpcc.9b06388
J. Phys. Chem. C 2019, 123, 24705−24713

reorganization energy in the aggregation state and checked the intermolecular interactions.

Based on the crystal structure of TAP−QCN, several dimers are investigated and intermolecular interactions are analyzed by the IGM method (as shown in Figure 7). In addition, the intermolecular interaction energy is decomposed based on the AMBER force field as shown in Table 3. It is found that the intermolecular interactions in dimer-2 and dimer-3 are both very weak, while they are the strongest in dimer-4. By a detailed analysis, we found that the interaction mainly comes from the dispersion between two molecules. In addition, $\pi-\pi$ interactions can be found in dimer-4, although the overlap between conjugated units is quite small. The $\pi-\pi$ interaction can also be found in dimer-1, while it mainly comes from the interaction of benzene rings in the donor. The $\pi-\pi$ interaction could inhibit the rotation of donor groups from low-frequency vibration modes and thus reduced the contribution to the reorganization energy from low-frequency modes. The electrostatic, repulsion, and dispersive energies in dimer-6 are relatively balanced, and moderate interaction is generated. Based on the IGM analysis, we can find that there is significant hydrogen-bond (H-bond) interaction in dimer-6. Are dimers such as dimer-6 with hydrogen bonds responsible for emission? The transition properties of dimer-6 and dimer-4 (with strong interaction energy) are analyzed (see Figure S2). It is found that the charge transfer during transition only occurs in one molecule, which indicates that dimers are not responsible for emission.

Table 3. Intermolecular Interaction Energy Including Electronic, Repulsion, and Dispersion Interactions in Several Dimers Extracted from the Crystal Structure

dimer	electrostatic	repulsion	dispersion	total (kJ/mol)
dimer-1	−2.73	5.87	−40.74	−37.59
dimer-2	−0.27	36.23	−44.24	−8.27
dimer-3	1.33	0.93	−5.99	−3.73
dimer-4	0.18	35.17	−95.33	−59.98
dimer-5	−2.28	10.47	−27.21	−19.02
dimer-6	−24.11	37.02	−43.02	−30.12
dimer-7	−10.12	10.83	−23.04	−22.33

By a detailed analysis on the vibration modes and the H-bond interaction, we find that the hydrogen atom that forms a H-bond with the nitrogen atom also contributes to the C−H stretching vibration mode that shows up in the aggregation state. We think that the enhanced contribution to the reorganization energy of C−H stretching vibration modes should be induced by the H-bond interaction. To confirm the deduction that the C−H stretching mode has a close relationship with the hydrogen bond, a model without a hydrogen bond is designed and investigated. The model is designed based on the ONIOM model in Figure 1b, where the CN unit involved in the hydrogen bond is replaced with the hydrogen atom (see Figure S3). Then, the optimization is performed, and the HR factor and reorganization energy are analyzed (see Figure S4). It is found that the HR factors are mainly contributed by low-frequency and moderate-frequency modes (such as HR = 0.22 and 0.16), and they mainly correspond to the rotation of the donor and conjugate chains as well as the C═C and the C−N stretching vibrations. More importantly, we found that the C−H stretching mode at high frequency shows little contribution to the HR factors and the reorganization energy, which is quite different from that with hydrogen bond. Thus, we think that the hydrogen bond plays an important role in the enlarged contribution of C−H stretching vibration modes to the reorganization. If we can avoid the formation of H-bonds in the aggregation state by molecular design or other crystal engineering, there will be no contribution to the reorganization energy from C−H stretching modes. The nonradiative rate will be effectively reduced and a high fluorescent efficiency could be obtained. Of course, the reorganization energy except for the contribution of the C−H stretching mode in the aggregation state is also larger than that in toluene, which mainly comes from the enhanced contribution from moderate-frequency modes (at about 1500 cm^{-1}). If these vibration modes can be effectively suppressed, the nonradiative rate could be further decreased.

Some other photophysical properties of the molecule without hydrogen bonds are also investigated. From the energy levels of excited states (see Figure S5), we can find that the excited energy of S_1 and T_1 are both decreased a little. The energy gap (0.14 eV) between S_1 and T_1 is a little larger than that with hydrogen bond (0.11 eV). There is also a little variation of the transition orbitals (see Figure S6), where the LE component increases in S_1 and decreases in T_1. In addition, the SOC constant between S_1 and T_1 is increased to 0.202 cm^{-1} and the ISC rate is increased to 2.17×10^7 s^{-1} (see Table S2). The RISC rate is a little decreased because a larger energy gap between S_1 and T_1 is found for the molecule without hydrogen bonds. There is no significant change in the radiative rate. Typically, the internal conversion rate is decreased to 1.72×10^8 s^{-1} and the fluorescence efficiency is enhanced. This is consistent with our proposal that the fluorescence efficiency could be increased by eliminating the hydrogen bond.

4. CONCLUSIONS

In summary, the light-emitting properties of the TPA−QCN molecule in both toluene and in the aggregation state are investigated based on first-principles and QM/MM calculations. It is found that the energy gap between S_1 and T_1 in the aggregation state is much smaller than that in toluene. Besides, the SOC is enhanced and the RISC rates are increased, which confirms an effective RISC process in the aggregation state. Our calculation results indicate that the transition dipole moment of TPA−QCN in the aggregation state is almost the same as that in solution. Nevertheless, the energy of S_1 is lower, which is the reason that the fluorescent rate is decreased. In addition, the nonradiative rate is significantly increased. Both the decreased fluorescent rate and increased nonradiative rate induced ACQ. By analyzing the intermolecular interaction and the reorganization energy, we found that the C−H stretching vibration modes show about 16% contribution to the reorganization energy in the aggregation state, while little contribution is found in toluene. The enhanced contribution of the C−H stretching vibration modes is mainly induced by the intermolecular H-bond interaction formed in the aggregation state. Thus, we think that the fluorescent efficiency could be effectively improved by avoiding the formation of H-bonds in the aggregation state. A new mechanism for ACQ is proposed, and our results may help in the design of new types of NIR-TADF molecules.

DOI: 10.1021/acs.jpcc.9b06388
J. Phys. Chem. C 2019, 123, 24705−24713

■ ASSOCIATED CONTENT

Supporting Information

The Supporting Information is available free of charge on the ACS Publications website at DOI: 10.1021/acs.jpcc.9b06388.

Bond lengths, bond angles, and dihedral angles; electron distribution in transition orbitals; ONIOM model, HR factors, reorganization energies, energy levels, NTOs, radiative rate, and internal conversion rate of the system without hydrogen bonds (PDF)

■ AUTHOR INFORMATION

Corresponding Authors

*E-mail: ckwang@sdnu.edu.cn (C.-K.W.).
*E-mail: linll@sdnu.edu.cn (L.L.).

ORCID

Lili Lin: 0000-0002-5319-713X

Notes

The authors declare no competing financial interest.

■ ACKNOWLEDGMENTS

This work is supported by the National Natural Science Foundation of China (Grant nos. 11874242 and 11974216) and Shandong Provincial Natural Science Foundation, China (ZR2019MA056). The authors acknowledge the support of Taishan Scholar Project of Shandong Province and the Project funded by China Postdoctoral Science Foundation (Grant no. 2018M642689). The authors are very grateful to Professor Yi Luo, Zhigang Shuai, and Qian Peng for their helpful suggestions in our calculations and to Professor Yingli Niu for his great help in the usage of MOMAP.

■ REFERENCES

(1) Tang, C. W.; VanSlyke, S. A. Organic Electroluminescent Diodes. *Appl. Phys. Lett.* **1987**, *51*, 913−915.

(2) Uoyama, H.; Goushi, K.; Shizu, K.; Nomura, H.; Adachi, C. Highly Efficient Organic Light-Emitting Diodes from Delayed Fluorescence. *Nature* **2012**, *492*, 234.

(3) Zhang, Q.; Li, B.; Huang, S.; Nomura, H.; Tanaka, H.; Adachi, C. Efficient Blue Organic Light-Emitting Diodes Employing Thermally Activated Delayed Fluorescence. *Nat. Photon.* **2014**, *8*, 326.

(4) Wong, M. Y.; Zysman-Colman, E. Purely Organic Thermally Activated Delayed Fluorescence Materials for Organic Light-Emitting Diodes. *Adv. Mater.* **2017**, *29*, No. 1605444.

(5) Tao, Y.; Yuan, K.; Chen, T.; Xu, P.; Li, H.; Chen, R.; Zheng, C.; Zhang, L.; Huang, W. Thermally Activated Delayed Fluorescence Materials Towards the Breakthrough of Organoelectronics. *Adv. Mater.* **2014**, *26*, 7931−7958.

(6) Tanaka, H.; Shizu, K.; Nakanotani, H.; Adachi, C. Dual Intramolecular Charge-Transfer Fluorescence Derived from a Phenothiazine-Triphenyltriazine Derivative. *J. Phys. Chem. C* **2014**, *118*, 15985−15994.

(7) Wang, S.; Cheng, Z.; Song, X.; Yan, X.; Ye, K.; Liu, Y.; Yang, G.; Wang, Y. Highly Efficient Long-Wavelength Thermally Activated Delayed Fluorescence OLEDs Based on Dicyanopyrazino Phenanthrene Derivatives. *ACS Appl. Mater. Interfaces* **2017**, *9*, 9892−9901.

(8) Gan, L.; Gao, K.; Cai, X.; Chen, D.; Su, S.-J. Achieving Efficient Triplet Exciton Utilization with Large ΔE_{ST} and Nonobvious Delayed Fluorescence by Adjusting Excited State Energy Levels. *J. Phys. Chem. Lett.* **2018**, *9*, 4725−4731.

(9) Chen, J.-X.; Liu, W.; Zheng, C.-J.; Wang, K.; Liang, K.; Shi, Y.-Z.; Ou, X.-M.; Zhang, X.-H. Coumarin-Based Thermally Activated Delayed Fluorescence Emitters with High External Quantum Efficiency and Low Efficiency Roll-Off in the Devices. *ACS Appl. Mater. Interfaces* **2017**, *9*, 8848−8854.

(10) Cui, L. S.; Nomura, H.; Geng, Y.; Kim, J. U.; Nakanotani, H.; Adachi, C. Controlling Singlet-Triplet Energy Splitting for Deep-Blue Thermally Activated Delayed Fluorescence Emitters. *Angew. Chem., Int. Ed.* **2017**, *56*, 1571−1575.

(11) Gao, Y.-J.; Chen, W.-K.; Zhang, T.-T.; Fang, W.-H.; Cui, G. Theoretical Studies on Excited-State Properties of Au (Iii) Emitters with Thermally Activated Delayed Fluorescence. *J. Phys. Chem. C* **2018**, *122*, 27608−27619.

(12) Kim, J. H.; Yun, J. H.; Lee, J. Y. Recent Progress of Highly Efficient Red and near-Infrared Thermally Activated Delayed Fluorescent Emitters. *Adv. Opt. Mater.* **2018**, *6*, No. 1800255.

(13) Kim, D.-H.; D'aléo, A.; Chen, X.-K.; Sandanayaka, A. D. S.; Yao, D.; Zhao, L.; Komino, T.; Zaborova, E.; Canard, G.; Tsuchiya, Y.; et al. High-Efficiency Electroluminescence and Amplified Spontaneous Emission from a Thermally Activated Delayed Fluorescent near-Infrared Emitter. *Nat. Photon.* **2018**, *12*, 98−104.

(14) Jiang, J.; Xu, Z.; Zhou, J.; Hanif, M.; Jiang, Q.; Hu, D.; Zhao, R.; Wang, C.; Liu, L.; Ma, D.; et al. Enhanced Pi Conjugation and Donor/Acceptor Interactions in Dad Type Emitter for Highly Efficient near-Infrared Organic Light-Emitting Diodes with an Emission Peak at 840 Nm. *Chem. Mater.* **2019**, *31*, 6499−6505.

(15) Yuan, Y.; Hu, Y.; Zhang, Y. X.; Lin, J. D.; Wang, Y. K.; Jiang, Z. Q.; Liao, L. S.; Lee, S. T. Over 10% EQE near-Infrared Electroluminescence Based on a Thermally Activated Delayed Fluorescence Emitter. *Adv. Funct. Mater.* **2017**, *27*, No. 1700986.

(16) Wang, S.; Yan, X.; Cheng, Z.; Zhang, H.; Liu, Y.; Wang, Y. Highly Efficient near-Infrared Delayed Fluorescence Organic Light Emitting Diodes Using a Phenanthrene-Based Charge-Transfer Compound. *Angew. Chem., Int. Ed.* **2015**, *54*, 13068−13072.

(17) Wang, S.; Miao, Y.; Yan, X.; Ye, K.; Wang, Y. A Dibenzo [a, c] Phenazine-11, 12-Dicarbonitrile (DBPzDCN) Acceptor Based Thermally Activated Delayed Fluorescent Compound for Efficient near-Infrared Electroluminescent Devices. *J. Mater. Chem. C* **2018**, *6*, 6698−6704.

(18) Xue, J.; Liang, Q.; Wang, R.; Hou, J.; Li, W.; Peng, Q.; Shuai, Z.; Qiao, J. Highly Efficient Thermally Activated Delayed Fluorescence Via J-Aggregates with Strong Intermolecular Charge Transfer. *Adv. Mater.* **2019**, *31*, No. 1808242.

(19) Li, C.; Duan, R.; Liang, B.; Han, G.; Wang, S.; Ye, K.; Liu, Y.; Yi, Y.; Wang, Y. Deep-Red to near-Infrared Thermally Activated Delayed Fluorescence in Organic Solid Films and Electroluminescent Devices. *Angew. Chem., Int. Ed.* **2017**, *56*, 11525−11529.

(20) Fan, D.; Yi, Y.; Li, Z.; Liu, W.; Peng, Q.; Shuai, Z. Solvent Effects on the Optical Spectra and Excited-State Decay of Triphenylamine-Thiadiazole with Hybridized Local Excitation and Intramolecular Charge Transfer. *J. Phys. Chem. A* **2014**, *119*, 5233−5240.

(21) Lin, L.; Wang, Z.; Fan, J.; Wang, C. Theoretical Insights on the Electroluminescent Mechanism of Thermally Activated Delayed Fluorescence Emitters. *Org. Electron.* **2017**, *41*, 17−25.

(22) Fan, J.; Zhang, Y.; Zhang, K.; Lin, L.; Wang, C.-K. Strategy to modulate the singlet-triplet energy gap for spiro-based thermally activated delayed fluorescence molecules. *J. Lumin.* **2019**, *209*, 372−378.

(23) Fan, J.; Zhang, Y.; Zhang, K.; Liu, J.; Jiang, G.; Lin, L.; Wang, C.-K. Effects of Intramolecular and Intermolecular Interactions on Excited State Properties of Two Isomeric Cu Complexes with AIE and TADF Mechanisms in Solid Phase: A QM/MM Study. *Org. Electron.* **2019**, *71*, 113−122.

(24) Chung, L. W.; Sameera, W.; Ramozzi, R.; Page, A. J.; Hatanaka, M.; Petrova, G. P.; Harris, T. V.; Li, X.; Ke, Z.; Liu, F.; et al. The Oniom Method and Its Applications. *Chem. Rev.* **2015**, *115*, 5678−5796.

(25) Zhang, Y.; Ma, H.; Wang, S.; Li, Z.; Ye, K.; Zhang, J.; Liu, Y.; Peng, Q.; Wang, Y. Supramolecular Structure-Dependent Thermally-Activated Delayed Fluorescence (TADF) Properties of Organic Polymorphs. *J. Phys. Chem. C* **2016**, *120*, 19759−19767.

(26) Wang, B.; Wang, X.; Wang, W.; Liu, F. Exploring the Mechanism of Fluorescence Quenching and Aggregation-Induced Emission of a Phenylethylene Derivative by QM (CASSCF and

DOI: 10.1021/acs.jpcc.9b06388
J. Phys. Chem. C 2019, 123, 24705−24713

TDDFT) and ONIOM (QM:MM) Calculations. *J. Phys. Chem. C* **2016**, *120*, 21850−21857.
(27) Lin, L.; Fan, J.; Wang, C.-K. Theoretical Perspective for Internal Quantum Efficiency of Thermally Activated Delayed Fluorescence Emitter in Solid Phase: A QM/MM Study. *Org. Electron.* **2017**, *51*, 349−356.
(28) Fan, J.; Zhang, Y.; Zhou, Y.; Lin, L.; Wang, C.-K. Excited State Properties of a Thermally Activated Delayed Fluorescence Molecule in Solid Phase Studied by Quantum Mechanics/Molecular Mechanics Method. *J. Phys. Chem. C* **2018**, *122*, 2358−2366.
(29) Fan, J.; Lin, L.; Wang, C.-K. Excited State Properties of Non-Doped Thermally Activated Delayed Fluorescence Emitters with Aggregation-Induced Emission: A QM/MM Study. *J. Mater. Chem. C* **2017**, *5*, 8390−8399.
(30) Frisch, M. J.; Trucks, G. W.; Schlegel, H. B.; Scuseria, G. E.; Robb, M. A.; Cheeseman, J. R.; Scalmani, G.; Barone, V.; Petersson, G. A.; Nakatsuji, H.. et al.*Gaussian 16*, revision A.03, Gaussian Inc.: Wallingford, CT, 2016.
(31) Tao, Y.; Yuan, K.; Chen, T.; Xu, P.; Li, H.; Chen, R.; Zheng, C.; Zhang, L.; Huang, W. Thermally Activated Delayed Fluorescence Materials Towards the Breakthrough of Organoelectronics. *Adv. Mater.* **2014**, *26*, 7931−7958.
(32) Zhang, Q.; Li, B.; Huang, S.; Nomura, H.; Tanaka, H.; Adachi, C. Efficient Blue Organic Light-Emitting Diodes Employing Thermally Activated Delayed Fluorescence. *Nat. Photon.* **2014**, *8*, 326.
(33) Zhang, Q.; Kuwabara, H.; Potscavage, W. J., Jr.; Huang, S.; Hatae, Y.; Shibata, T.; Adachi, C. Anthraquinone-Based Intramolecular Charge-Transfer Compounds: Computational Molecular Design, Thermally Activated Delayed Fluorescence, and Highly Efficient Red Electroluminescence. *J. Am. Chem. Soc.* **2014**, *136*, 18070−18081.
(34) Shuai, Z.; Peng, Q. Excited States Structure and Processes: Understanding Organic Light-Emitting Diodes at the Molecular Level. *Phys. Rep.* **2014**, *537*, 123−156.
(35) Peng, Q.; Yi, Y.; Shuai, Z.; Shao, J. Excited State Radiationless Decay Process with Duschinsky Rotation Effect: Formalism and Implementation. *J. Chem. Phys.* **2007**, *126*, No. 114302.
(36) Niu, Y.; Peng, Q.; Shuai, Z. Promoting-Mode Free Formalism for Excited State Radiationless Decay Process with Duschinsky Rotation Effect. *Sci. China, Ser. B: Chem.* **2008**, *51*, 1153−1158.
(37) Dalton, a Molecular Electronic Structure Program, Release Dalton2013, 2013, see http://daltonprogram.org.
(38) Lefebvre, C.; Rubez, G.; Khartabil, H.; Boisson, J.-C.; Contreras-García, J.; Hénon, E. Accurately Extracting the Signature of Intermolecular Interactions Present in the Nci Plot of the Reduced Density Gradient Versus Electron Density. *Phys. Chem. Chem. Phys.* **2017**, *19*, 17928−17936.
(39) Lu, T.; Chen, F. Multiwfn: A Multifunctional Wavefunction Analyzer. *J. Comput. Chem.* **2012**, *33*, 580−592.
(40) Pan, Y.; Li, W.; Zhang, S.; Yao, L.; Gu, C.; Xu, H.; Yang, B.; Ma, Y. High Yields of Singlet Excitons in Organic Electroluminescence through Two Paths of Cold and Hot Excitons. *Adv. Opt. Mater.* **2014**, *2*, 510−515.
(41) Chen, R.; Tang, Y.; Wan, Y.; Chen, T.; Zheng, C.; Qi, Y.; Cheng, Y.; Huang, W. Promoting Singlet/Triplet Exciton Transformation in Organic Optoelectronic Molecules: Role of Excited State Transition Configuration. *Sci. Rep.* **2017**, *7*, No. 6225.
(42) Gorse, A. D.; Pesquer, M. Intramolecular Charge Transfer Excited State Relaxation Processes in Para-Substituted N,N-Dimethylaniline: A Theoretical Study Including Solvent Effects. *J. Phys. Chem. A* **1995**, *99*, 4039−4049.
(43) Reimers, J. R. A Practical Method for the Use of Curvilinear Coordinates in Calculations of Normal-Mode-Projected Displacements and Duschinsky Rotation Matrices for Large Molecules. *J. Chem. Phys.* **2001**, *115*, 9103−9109.

DOI: 10.1021/acs.jpcc.9b06388
J. Phys. Chem. C 2019, 123, 24705−24713